

Density functional study of closed-shell attraction on $X(ML)_3^+$ ($X=O, S, Se$; $M=Au, Ag, Cu$) systems

Abstract With the help of quantum mechanical calculations, we have examined the series of central system $X(ML)_3^+$ ($X=O, S, Se$; $M=Au, Ag, Cu$). Using a scalar-relativistic density functional approach, we studied the geometry structures, Mulliken populations and charges of the systems. Structure parameters of the experimental systems are reproduced well with $X\alpha$ method. The metallophilic interaction energy is analyzed and decomposed. For the systems with different central atoms and different metal atoms, the nature of the metallophilic attraction interaction is analyzed.

Keywords Closed-shell · Metallophilic interaction · Density functional · Mulliken population

Introduction

The existence of metal...metal contacts shorter than the sum of the van der Waals radii between d^{10} transition metal complexes have been detected in recent years in a large number of crystal structures [1].

These interactions are weaker than ionic bond and covalent bond, and stronger than van der Waals bond, can achieve strength qualitatively comparable with strong hydrogen bond. These interactions are important in determining the structures of many of these complexes [2, 3]. The stabilization energies of aurophilic interaction vary from 29 to 46 kJ/mol [1].

The role of strong closed-shell attraction (called “aurophilic interaction”) in their stability and structure is well

established. Many centered gold clusters such as $[C(AuL)_5]^+$, $[C(AuL)_6]^{2+}$, $[N(AuL)_5]^{2+}$, $[P(AuL)_5]^{2+}$, and $[P(AuL)_6]^{3+}$ have been described [4–7], and all have in common the presence of $Au(I)...Au(I)$ interactions of ca. 3 Å.

Although the chemistry of carbon-, nitrogen-, phosphorus-, or arsenic-centered species has developed rapidly, the corresponding chemistry of chalcogen derivatives is still growing. $\{Se(AuL)_3^+\}$ [2, 8–10], $\{O(AuL)_3^+\}$ [7, 11, 12], $\{S(AuL)_4\}^{2+}$ [9], were prepared one after the other.

Theoretical work in this area was pioneered by Pyykkö, who used HF and MP2 methods to study the aurophilicity in $[XAuPH_3]_2$ dimers, where X is one from a range of groups such as the halogens, methyl and SCH_3 [13, 14]. Pyykkö's calculations were extremely revealing. Aurophilicity is due to electron correlation (or dispersion forces) and also that the attraction is strengthened by relativistic effects. Although relativistic effects are important but not dominant. Magnko et al. [15] confirmed what Pyykkö et al. had discovered previously, that the strength of the metallophilic interaction in $[ClMPH_3]_2$ ($M=Cu, Ag, Au$) increases as the metal becomes heavier, by approximately 50% from Cu to Au. O'Grady and Kaltsoyannis studied the same free dimer [16], and concluded that cuprophilic interaction is the strongest, argentophilic interaction is the weakest. Pyykkö and Tamm [17] have studied the central systems by using Hartree–Fock (HF) and perturbation theory (MP2) method. Later, Pyykkö et al. [18] studied the A-frame system $S(MPH_3)_2$ ($M=Cu, Ag, Au$) at levels up to CCSD(T). In such system, aurphilic interaction is the strongest, the cuprophilic interaction is the weakest. For most central atom systems, there is no good method to analyze the metallophilicity.

We therefore felt that there was scope to explore metallophilicity in these groups $[X(ML)_3]^+$ ($X=O, S, Se$; $M=Au, Ag, Cu$) by using DFT level. While we acknowledge that, as Magnko et al. note, “van der Waals like attraction

H. Fang · S.-G. Wang (✉)
School of Chemistry and Chemical Technology,
Shanghai Jiao Tong University,
Shanghai 200240, China
e-mail: sgwang@sjtu.edu.cn

cannot be reliably described with current DFT techniques fare schemes” we were interested to see how DFT techniques fare in the metallophilicity arena. The calculated structural data can be compared with a large class of experimentally known compounds. For the different central atoms and different metal atoms, the structural parameters and the metallophilic energies are compared.

Computational details

All calculations were performed using the Amsterdam density functional (ADF 2004) package initially developed by Baerends et al. [19]. Four different exchange-correlation DF were applied: (1) the simple local $X\alpha$ exchange potential by Slater [20–22], with parameter $\alpha=0.7$; (2) the local correlation-corrected version developed by Vosko, Wilk and Nusair (VWN) in 1980 [23]; (3) the nonlocal gradient-corrected exchange potential of Becke (B) of 1988 [24] together with nonlocal gradient-corrected correlation potential of Perdew (P) of 1986 [25]; (4) the generalized gradient approach of Perdew and Wang (PW91) [26].

In order to reduce the calculational expenses, the inner core shells were frozen [27]. $[1s^2-4f^{14}]$ core for Au, $[1s^2-4p^6]$ core for Ag, $[1s^2-3p^6]$ core for Cu, $[1s^2]$ core for O, $[1s^2-2p^6]$ core for S, $[1s^2-3d^{10}]$ core for Se were frozen. The atomic core orbitals were calculated by the Dirac method and then kept unrelaxed in the molecules.

Relativistic effect was particularly important to gold atom and auophilic interaction. We used the scalar relativistic zeroth order regular approximation (ZORA) [28–31] which averages over spin-orbit splittings. Spin-orbit effects are expected to be unimportant to Au(I) systems. For Ag and Cu atoms, the relativistic effects were also considered.

High quality triple- ξ , Slater-type plus two polarization (TZ2P) orbital basis sets were used for the valence shells of all atoms.

In the experimental structures, the ligand L is typically triphenylphosphine $-P(C_6H_5)_3$. For computational efficiency, it is replaced by the unsubstituted phosphine group $-PH_3$. This substitution has been found to have little influence on the X–M and M–P bond lengths [32, 33]. For the tripodes molecules $X(ML)_3^+$ ($X=O, S, Se$; $M=Au, Ag, Cu$), C_{3v} symmetry was assumed. Geometry structure is illustrated in Fig. 1.

Results and discussions

Structures

Crystalline $O(AuP(^iPr)_3)_3^+$ [34], $S(AuP(Ph)_3)_3^+$ [35], $Se(AuPPh_3)_3^+$ [36] have been reported. The small Au–X–

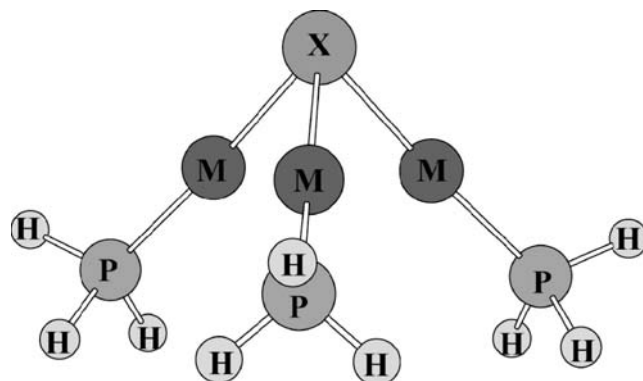


Fig. 1 Structure of the studied system $X(ML)_3^+$ ($X=O, S, Se$; $M=Au, Ag, Cu$)

Au angles seem to indicate significant Au...Au attraction, although nonbonding interactions between PR_3 ligands also play a role. For the electronic structure investigations, the complex $X(AuL)_3^+$ ($X=O, S, Se$) has been taken to model experimentally available cations which contain larger phosphine substituents [34–36].

The results of the geometry optimizations of the $X(AuL)_3^+$ ($X=O, S, Se$) were reported in Table 1. A full geometry optimization was carried out for $X(AuL)_3^+$ ($X=O, S, Se$), imposing C_{3v} symmetry. The Au...Au distance, Au–X, Au–P bond and the Au–X–Au angle were shown in Table 1.

Table 1 Main geometric parameters of $X(AuPH_3)_3^+$ ($X=O, S, Se$) (basis set: TZ2P, bond distance in pm, angle in degree)

System	Method	$R_{Au...Au}$	R_{Au-X}	R_{Au-P}	$\theta_{Au-X-Au}$
$O(AuPH_3)_3^+$	HF ¹⁷	354.8	204.8	232.3	120.0
	MP2 ¹⁷	298.1	202.9	224.8	94.6
	$X\alpha$	320.0	200.0	219.0	106.3
	VWN	313.0	200.2	218.0	103.0
	BP	338.0	204.3	222.0	112.0
	PW91	347.0	203.8	222.0	116.9
	Exp ^a	319.8	203.0	222.8	103.7
$S(AuPH_3)_3^+$	HF ¹⁷	377.5	238.8	238.0	104.4
	MP2 ¹⁷	294.4	233.1	228.6	78.3
	$X\alpha$	301.0	230.0	225.0	81.5
	VWN	299.0	230.4	224.0	81.0
	BP	346.0	233.7	227.0	95.6
	PW91	366.0	233.0	227.0	103.5
	Exp ^b	310.0	232.0	226.0	84.0
$Se(AuPH_3)_3^+$	HF ³⁷	385.0	250.4	241.5	100.5
	MP2 ³⁷	297.5	246.5	232.5	74.2
	$X\alpha$	300.0	244.0	224.0	75.7
	VWN	298.0	244.2	223.0	75.4
	BP	308.0	249.6	228.0	76.3
	PW91	307.0	248.0	228.0	76.4
	Exp ^c	301.8	244.7	227.4	80.1

^aAverage structure of $O(AuP(^iPr)_3)_3^+$ of Ref [34]; ^bstructure of $S(AuP(Ph)_3)_3^+$ of Ref [35], ^cstructure of $Se(AuPPh_3)_3^+$ of Ref [36]

At first, we compare the fully optimized structures of the system $O(AuPH_3)_3^+$ in Table 1, as obtained by HF [17], MP2 [17] and several DF methods, and by experiment (on solid phases). As known, ab initio HF overestimated by 2 pm for Au–O bond, 9 pm for Au–P bond, 35 pm for Au...Au distance and 16° for Au–O–Au angle. With the correlation correction of MP2, both the Au...Au distance and the Au–O–Au angle reduce 56 pm and 25° , respectively. Compared the MP2 results to the experimental values, the Au–O and Au–P bonds come to an agreement with the experimental values within 2 pm. While the Au...Au distance and Au–O–Au angle are underestimated by about 12 pm and 9° . MP2 method can not be fit for such closed-shell systems [18]. Even high level MP4 and CCSD(T) have been applied, there were still deviations between theoretical and experimental data [18]. Compared calculated geometry parameters of $O(AuPH_3)_3^+$ molecule by using DF methods to experimental geometries, both of the BP and PW91 theoretical methods overestimate Au...Au distance by about 18–27 pm. The Au–O distance and Au–P distance obtained with BP and PW91 methods were underestimated by average 1 pm and 1 pm, respectively. While $X\alpha$ and VWN methods give the reliable structures. The Au...Au distance obtained by $X\alpha$ method is the closest to experimental value.

For $S(AuPH_3)_3^+$ molecule, HF [17] method overestimates the Au–S bond, Au–P bond, Au...Au distance and Au–S–Au angle for 7 pm, 12 pm, 67 pm and 20° , respectively. With the correlation correction of MP2 [17], both the Au–S and Au–P bonds are close to the experimental values, on the contrary, the Au...Au distance and Au–S–Au angle are underestimated the Au...Au distance for 16 pm and Au–S–Au angle for 6° . Compared the structure parameters of DF methods to the experimental values, BP and PW91 methods both overestimate Au–Au distance by 36 pm and 56 pm, Au–S distance by 1 and 2 pm, Au–P by 1 and 1 pm and underestimate Au–S–Au angle by 12° and 20° . The results with $X\alpha$ and VWN methods are all close and underestimate experimental values by 9 pm and 11 pm for Au...Au distance, 2.5° and 3° for Au–S–Au angle. $X\alpha$ method is better than VWN methods.

For $Se(AuPH_3)_3^+$ molecule, $X\alpha$ and VWN methods give similar results as MP2 [37] or experiment [36]. When nonlocal exchange and correlation corrections are added (BP, PW91), the Au...Au distance and Au–Se–Au angle increase by about 6 pm and 4° . For such closed-shell systems, $X\alpha$ is the most suitable methods to such systems. Recently, Autschbach et al. [33] studied the $C(AuL)_6^{2+}$ system by using DFT methods and drew the conclusion “the use of GGA functionals such as BP86 is state-of-the-art in DFT calculations of large molecules, and since we do not want to rely on a possible error cancellation within the local density approximation”. However, we have investigated the closed-

shell systems by means of DFT methods [38] and other many systems and found that local spin density potentials such as VWN and $X\alpha$ are superior to GGA functionals. So, Why current LDA-DFT can work on the closed-shell systems and why GGA potentials under estimated closed-shell interactions are still open questions.

The geometries of the tripodes molecules $X(MPH_3)_3^+$ ($X=O, S, Se; M=Ag, Cu$) are also fully optimized at the $X\alpha/TZ2P$ levels. The parameters of the structure are listed in Table 2.

The R_{X-M} and R_{M-P} data are plotted in Fig. 2. When the metal is the same, R_{X-M} increases very significantly as the central atomic number becomes bigger. Namely, R_{X-Au} varies with the central atomic electronegativity. When the central atom is the same, R_{X-M} varies along with the order: $R_{X-Ag} > R_{X-Au} > R_{X-Cu}$. By contrast, there is a contraction in R_{X-M} from Ag to Au within 5 pm. The relativistic bond length contraction in $X(MPH_3)_3^+$ ($X=O, S, Se; M=Ag, Cu$) system, the argument goes, will be larger when there is appreciable ns character to the bonding. The relativistic effect of Au atom is stronger than Ag. R_{X-Au} is shorter than R_{X-Ag} because of the relativistic bond length contraction.

Figure 2b shows the change of R_{M-P} for different X and M. When the metal is the same, the central atom also affected the R_{M-P} . The changeable order is: R_{M-P} ($X=S$) $> R_{M-P}$ ($X=Se$) $> R_{M-P}$ ($X=O$). The bond length contraction is originated from the relativistic effect for Se atom. When the central atom is the same, R_{Ag-P} is the biggest, while R_{Cu-P} is the smallest. The relativistic effect of Au atom is stronger than Ag. R_{Au-P} is shorter than R_{Ag-P} because of the relativistic bond length contraction.

As can be seen from the Mulliken charges given in Table 4, the M–X bond is certainly more ionic in the X^-M^+ sense than is the M–P (as expected given the relative electronegativity of X and P) [16]. Thus the R_{M-X} contraction should be less than that of R_{M-P} , as is indeed observed. Bowmaker et al. [39], involves changes in M–P backbonding. Relativistic effects destabilize valence d orbitals, and thus should enhance π back-donation from

Table 2 $X(ML)_3^+$ ($X=O, S, Se; M=Ag, Cu$): optimized structures (bond length in pm, angle in degree) at $X\alpha/TZ2P$ level

System	$R_{M...M}$	R_{X-M}	R_{M-P}	θ_{M-X-M}
$[O(AuPH_3)_3]^+$	320.0	200.0	219.0	106.3
$[O(AgPH_3)_3]^+$	343.0	200.5	227.0	117.9
$[O(CuPH_3)_3]^+$	306.0	179.0	212.0	117.4
$[S(AuPH_3)_3]^+$	301.0	230.0	225.0	81.5
$[S(AgPH_3)_3]^+$	298.0	234.8	237.0	78.9
$[S(CuPH_3)_3]^+$	284.0	214.6	217.0	83.0
$[Se(AuPH_3)_3]^+$	300.0	244.0	224.0	75.7
$[Se(AgPH_3)_3]^+$	301.0	246.0	234.0	75.6
$[Se(CuPH_3)_3]^+$	293.0	227.7	216.5	80.2

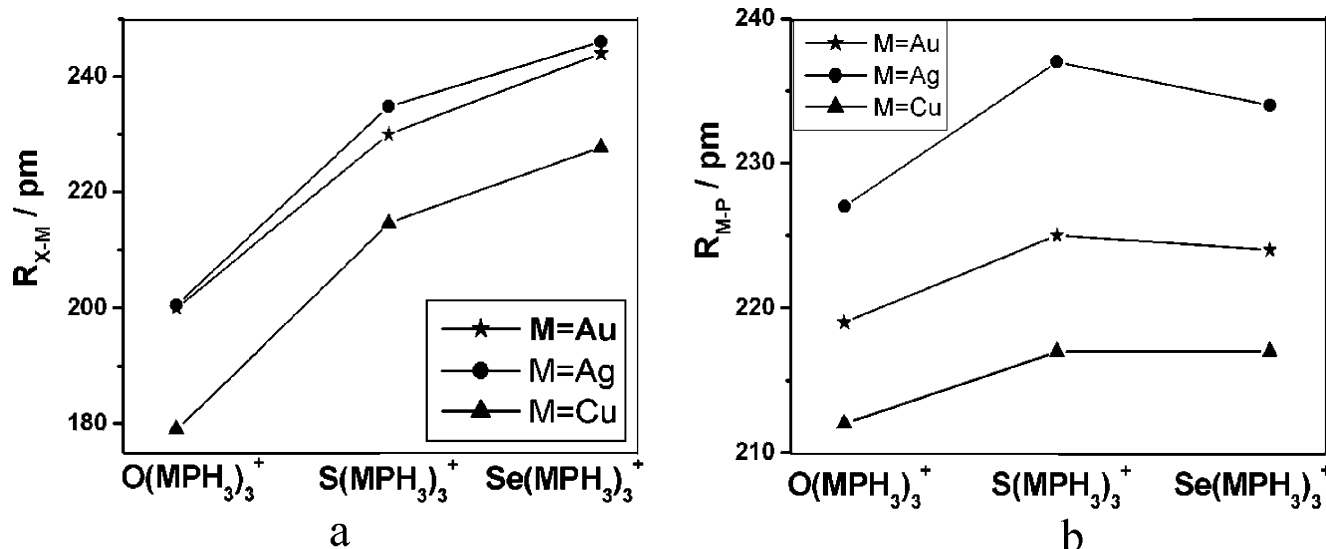


Fig. 2 R_{X-M} and R_{M-P} for $X(MPH_3)_3^+$ ($X=O, S, Se$; $M=$ Au, Ag, Cu)

the M nd orbitals to the PH_3 group, strengthening the M–P bond.

At last, the $M(I)...M(I)$ distance is compared (see Fig. 3). When the central atom is the same, the $R_{M...M}$ varies along the order: $R_{Ag...Ag} > R_{Au...Au} > R_{Cu...Cu}$. Since the relativistic effect of Au atom is important, there is a contraction from Ag to Au. But the bond length contraction is different with different central atom. The bigger electronegativity of the central atom is, the more bond length contraction is. Ziegler et al. [40] found that the relativistic bond length contraction decreased in the order $Au_2 > AuH > AuCl$, and noted “the smallness of relativistic effects in $AuCl$ compared to Au_2 and AuH , is probably due to the fact that this compound is much more ionic than the other two, so that the valence orbitals are largely concentrated on the Cl center, where

relativistic effects are substantially smaller than Au^{+} ”. When the metal is the same, the central atom can affect the $M...M$ distance. If the metal atom is Ag or Cu, the $R_{M...M}$ ($X=O$) $>R_{M...M}$ ($X=S$) $>R_{M...M}$ ($X=Se$); if the central atom is Au, the $R_{M...M}$ decreased following the raising of the central atom number.

Metallophilic interaction energy

For the $X(MPH_3)_3^+$ ($X=O, S, Se$; $M=$ Au, Ag, Cu) systems, since the metallophilic interaction exists, the geometry structure changed from D_{3h} symmetry to C_{3v} symmetry. The metallophilic interaction can be obtained by the following equation:

$$\Delta E_{M...M} = E_{C3v} - E_{D3h} \quad (1)$$

Changing from D_{3h} to C_{3v} structure, there is contained of hybridization forces at the central atom. We take XH_3^+ as a reference in which the hybridization forces of central X atom reducing the H–X–H angle from D_{3h} to C_{3v} . The differences of $M-X-M$ angle compared with H–X–H angle were defined as extra offset angles $\delta\theta_{M-H}$, $\delta\theta_{M-H} = \Delta\theta_{C3v-D3h}(MXM) - \Delta\theta_{C3v-D3h}(HXH)$ and are showed in Table 3.

We found that there existed a linear relationship between metallophilic interactions $\Delta E_{M...M}$ and extra offset angles $\delta\theta_{M-H}$ (see Fig. 4).

For the same metal atom, the metallophilic energy increases when the central atomic number increases. Namely, the metallophilic interaction increases corresponding to the decrease of the electronegativity of the central atom. When the central atom is S or Se, the metallophilic interaction between Au atoms is the strongest,

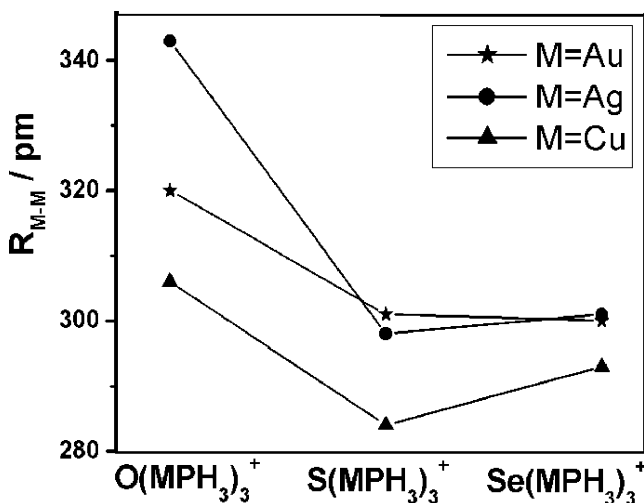


Fig. 3 R_{M-M} for $X(MPH_3)_3^+$ ($X=O, S, Se$; $M=$ Au, Ag, Cu)

Table 3 Angles of XH_3^+ and $X(ML)_3^+$ ($X=O, S, Se; M=Au, Ag, Cu$): optimized structures (angle in degree) and $\Delta\theta_{C3v-D3h}$ at $X\alpha/TZ2P$ level

Sym.	Angles		
	θ_{H-O-H}	θ_{H-S-H}	θ_{H-Se-H}
D_{3h}	120.0	120.0	120.0
C_{3v}	114.7	92.7	91.0
$\Delta\theta_{C3v-D3h}$	-5.3	-27.3	-29.0
	$\theta_{Au-O-Au}$	$\theta_{Au-S-Au}$	$\theta_{Au-Se-Au}$
D_{3h}	120.0	120.0	120.0
C_{3v}	106.3	81.5	75.7
$\Delta\theta_{C3v-D3h}$	-13.7	-38.5	-44.3
$\delta\theta_{Au-H}$	-8.4	-11.2	-15.3
$\Delta E_{Au...Au}$	-7.13	-47.09	-66.63
	$\theta_{Ag-O-Ag}$	$\theta_{Ag-S-Ag}$	$\theta_{Ag-Se-Ag}$
D_{3h}	120.0	120.0	120.0
C_{3v}	117.9	78.9	75.6
$\Delta\theta_{C3v-D3h}$	-2.1	-41.1	-44.4
$\delta\theta_{Ag-H}$	3.2	-13.8	-15.4
$\Delta E_{Ag...Ag}$	-0.35	-25.78	-41.19
	$\theta_{Cu-O-Cu}$	$\theta_{Cu-S-Cu}$	$\theta_{Cu-Se-Cu}$
D_{3h}	120.0	120.0	120.0
C_{3v}	117.4	83.0	80.2
$\Delta\theta_{C3v-D3h}$	-2.6	-37.0	-39.8
$\delta\theta_{Cu-H}$	2.7	-9.7	-10.8
$\Delta E_{Cu...Cu}$	0.40	-33.09	-44.27

$$\delta\theta_{M-H} = \Delta\theta_{C3v-D3h}(MXM) - \Delta\theta_{C3v-D3h}(HXH)$$

while the interaction between Ag is the weakest among Au, Ag and Cu atoms. However, O’Grady and Kaltsoyannis [16] studied the $[Cl-M-PH_3]_2$ and concluded that the cuprophilic interaction is the strongest, argentophilic interaction is the weakest. For the $O(MPH_3)_3^+$ ($M=Au, Ag, Cu$), $\Delta E_{Au...Au} > \Delta E_{Ag...Ag} > \Delta E_{Cu...Cu}$. In the system, the metallophilic interaction energy is small, especially for $M=Cu$.

Mulliken populations and charges of $X(MPH_3)_3^+$ ($X=O, S, Se; M=Au, Ag, Cu$)

Thirdly, we will discuss the charge distribution of $X(MPH_3)_3^+$ ($X=O, S, Se; M=Au, Ag, Cu$) by means of a Mulliken population analysis. Corresponding results are shown in Table 4.

From Table 4, we can see that the effective Mulliken charges on the Au atoms of $X(AuPH_3)_3^+$ systems vary between 0.06+ and 0.28+. At the same time, there are 0.5 to 0.6 electron holes in the Au5d shell, 0.9 to 1.0 e in the Au6s and 0.3 to 0.4 e in the Au6p valence shells. From the data, the PH_3 ligand transfers 0.3–0.4 electronic charges on to the Au atom, so that the gold atoms carry only very small positive effective charges. The small effective charges on Au seem to enhance the $Au(I)...Au(I)$ attraction [38]. Au 5d orbital can make a definite, though small, contribution to the $Au...Au$ bond. The radial bonds of the gold cluster (to the central atom as well as to the outer ligands) lead to a further reduction in the Au5d population, thereby improving the possibility of the aurophilic interaction. These results show that the 5d shell is not completely closed and that it thus may contribute to the closed-shell interaction. For the other system $X(MPH_3)_3^+$ ($X=O, S, Se; M=Ag, Cu$), since the Ag4d and Cu3d are not completely closed, then the argentophilic and cuprophilic interactions exist. Namely, the small electron holes in Au5d, Ag4d and Cu3d are very important to the closed-shell interaction.

Bond energy decomposition

According to the theory of Ziegler [41], the bond energy can be split up into two parts [42, 43]. One is the “steric interaction energy (E_{ster})” which comes from the electrostatic interaction

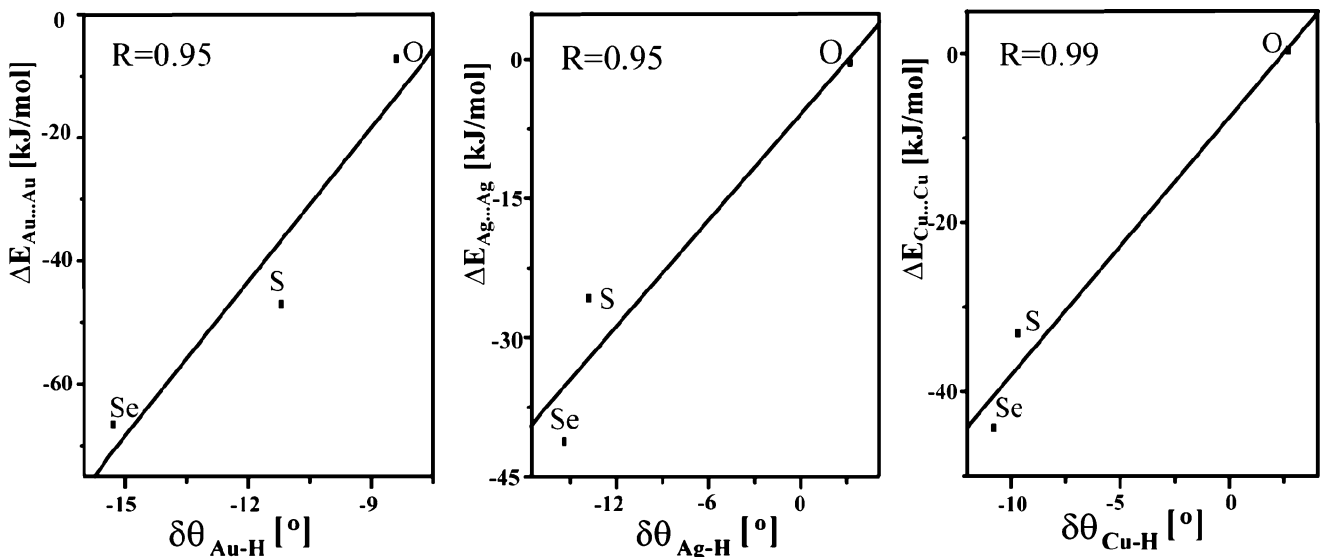


Fig. 4 Metallophilic interactions $\Delta E_{M...M}$ and extra offset angles $\delta\theta_{M-H}$, ($M=Au, Ag$ and Cu)

Table 4 Mulliken populations and charges of $X(\text{MPH}_3)_3^+$ ($X=\text{O}, \text{S}, \text{Se}; M=\text{Au}, \text{Ag}, \text{Cu}$) at $X\alpha/\text{TZ2P}$ level

System	Valence shells						
	Au6s	Au6p	Au5d	Au5f	Q_{Au}	Q_X	Q_{PH3}
$\text{O}(\text{AuPH}_3)_3^+$	0.99	0.31	-0.62	0.04	0.28	-0.92	0.36
$\text{S}(\text{AuPH}_3)_3^+$	1.02	0.41	-0.52	0.03	0.06	-0.23	0.35
$\text{Se}(\text{AuPH}_3)_3^+$	1.01	0.41	-0.53	0.03	0.08	-0.26	0.34
	Ag5s	Ag5p	Ag4d	Ag4f	Q_{Ag}	Q_X	Q_{PH3}
$\text{O}(\text{AgPH}_3)_3^+$	0.77	0.19	-0.32	0.03	0.33	-1.10	0.37
$\text{S}(\text{AgPH}_3)_3^+$	0.83	0.37	-0.26	0.03	0.03	-0.20	0.37
$\text{Se}(\text{AgPH}_3)_3^+$	0.86	0.34	-0.26	0.02	0.04	-0.20	0.36
	Cu4s	Cu4p	Cu3d	Cu3f	Q_{Cu}	Q_X	Q_{PH3}
$\text{O}(\text{CuPH}_3)_3^+$	0.71	0.29	-0.33	0.02	0.31	-1.16	0.41
$\text{S}(\text{CuPH}_3)_3^+$	0.75	0.51	-0.23	0.01	-0.04	-0.14	0.42
$\text{Se}(\text{CuPH}_3)_3^+$	0.75	0.49	-0.22	0.01	-0.03	-0.14	0.41

(E_{ele}) between the fragments (with unchanged electron densities) and the Pauli exchange repulsion (E_{Pauli}) due to the antisymmetry requirement raising the energy when occupied fragment orbitals overlap. The other is the “orbital interaction energy” (E_{orb}) due to quantum mechanical interference and orbital relaxation from the initial fragment states to the final molecular states. The orbital interaction contains charge transfer contributions (mixing of occupied orbitals on one fragment and virtual orbitals on the other fragment) and polarization contributions (mixing of occupied and virtual orbitals on the fragment itself).

$$E_{\text{tot}} = E_{\text{ster}} + E_{\text{orb}} = E_{\text{Pauli}} + E_{\text{ele.}} + E_{\text{orb}} \quad (2)$$

The Au...Au bonding energy for the $X(\text{MPH}_3)_3^+$ ($X=\text{O}, \text{S}, \text{Se}; M=\text{Au}, \text{Ag}, \text{Cu}$) at the $X\alpha$ level are broken down following the Eq. (2) and given in Table 5. The ΔE_{tot} is the metallophilic interaction of the systems by the geometry changing from D_{3h} to C_{3v} . For $\text{O}(\text{AuPH}_3)_3^+$ system, the Pauli repulsion energy (E_{Pauli}) decreased 91.13 kJ/mol, electrostatic interaction energy ($E_{\text{ele.}}$) increased 2.52 kJ/mol, orbital interaction energy (E_{orb}) increased 81.48 kJ/mol. The aurophilic interaction energy ΔE becomes to -7.13 kJ/mol. The sum of the electrostatic interaction and the orbital interaction increased 84.00 kJ/mol and were less than the decreased of the pauli interaction. In the $\text{O}(\text{AuPH}_3)_3^+$ molecule, the pauli interaction energy converted into aurophilic interaction. For $X(\text{AuPH}_3)_3^+$ ($X=\text{O}, \text{S}, \text{Se}$) system, the nature of aurophilic interaction originated from the pauli repulsion when the structure from D_{3h} to C_{3v} . ΔE_{Pauli} increases when the central atomic number increases, which made the aurophilic interaction energy increase from O, S to Se.

For the $X(\text{AgPH}_3)_3^+$ ($X=\text{O}, \text{S}, \text{Se}$) systems, the argentophilic interaction energies are converted from the decrease of the Pauli interaction. When the central atom becomes heavier, the argentophilic interaction increases at the same time.

The cuprophilic interaction energies for $X(\text{CuPH}_3)_3^+$ ($X=\text{O}, \text{S}, \text{Se}$) are listed in Table 5 and plotted in Fig. 4. The Pauli repulsion energy (E_{Pauli}) increases 7.55 kJ/mol from D_{3h} to C_{3v} in $\text{S}(\text{CuPH}_3)_3^+$. The electrostatic interaction ($E_{\text{ele.}}$) decreases 74.9 kJ/mol, the orbital interaction energy (E_{orb}) increases 34.26 kJ/mol, the sum of E_{ster} and E_{orb} comes to -33.09 kJ/mol. The nature of the cuprophilic interaction is electrostatic interaction in $\text{S}(\text{CuPH}_3)_3^+$ system.

For the $\text{Se}(\text{CuPH}_3)_3^+$ molecule, the Pauli repulsion energy (E_{Pauli}) decreases 81.84 kJ/mol from D_{3h} to C_{3v} . Electrostatic

Table 5 Bonding energy (ΔE , in kJ/mol) decomposition of $X(\text{MPH}_3)_3^+$ ($X=\text{O}, \text{S}, \text{Se}; M=\text{Au}, \text{Ag}, \text{Cu}$) at $X\alpha/\text{TZ2P}$ level

ΔE	Systems		
	$\text{O}(\text{AuPH}_3)_3^+$	$\text{S}(\text{AuPH}_3)_3^+$	$\text{Se}(\text{AuPH}_3)_3^+$
E_{Pauli}	-91.13	-202.37	-221.31
$E_{\text{ele.}}$	2.52	18.56	7.76
E_{ster}	-88.61	-183.81	-213.55
E_{orb}	81.48	136.72	146.92
E_{tot}	-7.13	-47.09	-66.63
	$\text{O}(\text{AgPH}_3)_3^+$	$\text{S}(\text{AgPH}_3)_3^+$	$\text{Se}(\text{AgPH}_3)_3^+$
E_{Pauli}	-27.87	-192.10	31.18
$E_{\text{ele.}}$	6.77	-9.57	-94.70
E_{ster}	-21.10	-201.67	-63.52
E_{orb}	20.75	175.89	22.33
E_{tot}	-0.35	-25.78	-41.19
	$\text{O}(\text{CuPH}_3)_3^+$	$\text{S}(\text{CuPH}_3)_3^+$	$\text{Se}(\text{CuPH}_3)_3^+$
E_{Pauli}	7.15	7.55	-81.84
$E_{\text{ele.}}$	1.09	-74.90	-17.89
E_{ster}	8.24	-67.35	-99.73
E_{orb}	-7.84	34.26	55.46
E_{tot}	0.40	-33.09	-44.27

E_{Pauli} : Pauli repulsion; $E_{\text{ele.}}$: electrostatic energy; E_{ster} : steric interaction which is the sum of E_{Pauli} and $E_{\text{ele.}}$; E_{orb} : orbital relaxation energy; E_{tot} : total bond energy. ΔE : energy difference between in C_{3v} and in D_{3h} structures

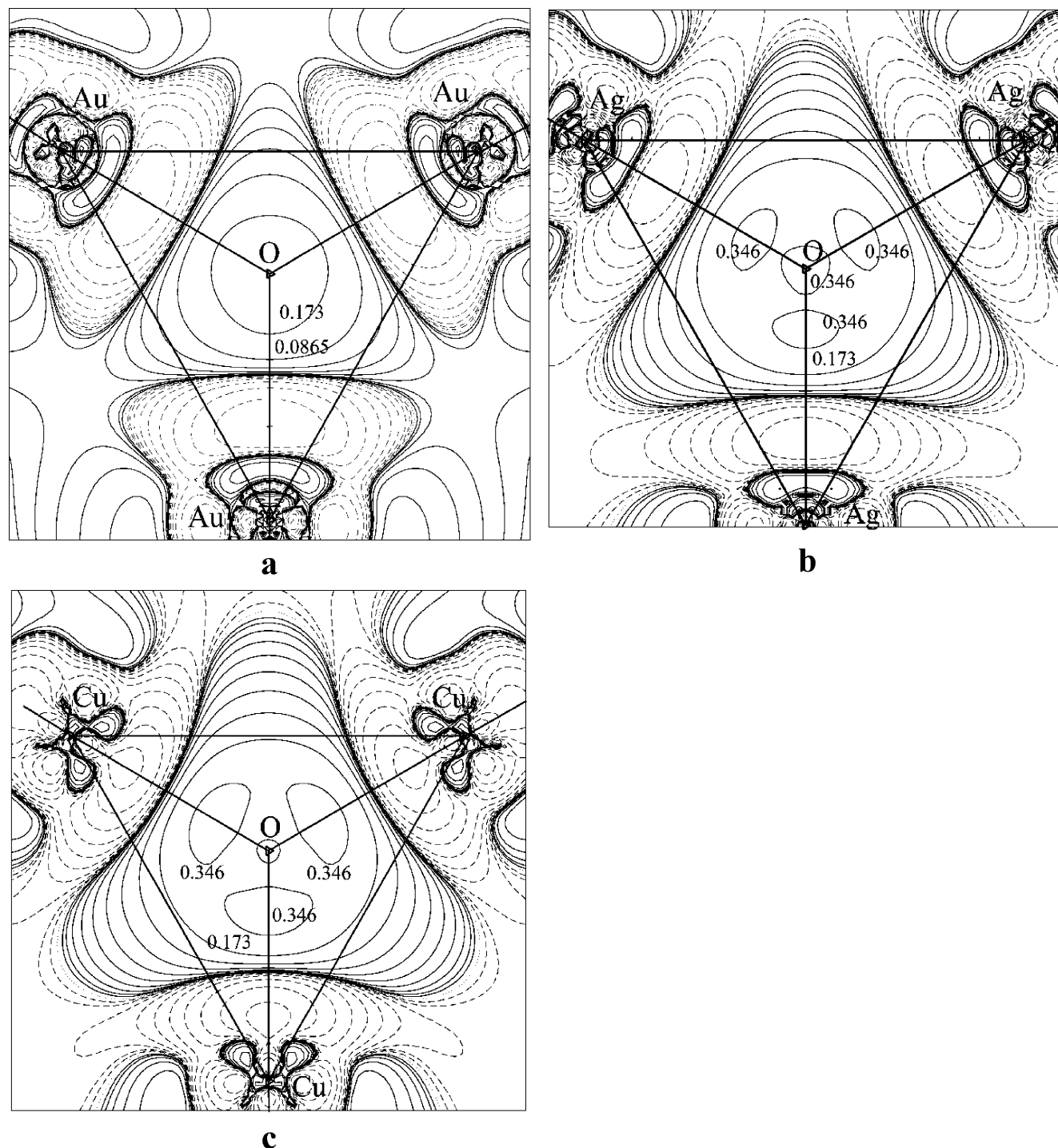


Fig. 5 Electron density difference $\Delta\rho$ ($e/\text{\AA}^3$) plots at $X\alpha/\text{TZ2P}$ level, **a**: $\text{O}(\text{AuPH}_3)_3^+$; **b**: $\text{O}(\text{AgPH}_3)_3^+$; **c**: $\text{O}(\text{CuPH}_3)_3^+$; along the plane of 3 Aus. Contour line values are $\pm 0.01 \times 2^n e\text{\AA}^{-3}$ ($n=0, 1, 2, \dots$); negative contour lines are dashed

interaction energy ($E_{\text{ele.}}$) decreases 17.89 kJ/mol, orbital interaction energy (E_{orb}) increases 55.46 kJ/mol, the sum of $E_{\text{ster.}}$ and E_{orb} decreases 44.27 kJ/mol. The decrease Pauli repulsion converted into cuprophilic interaction. In the $\text{Se}(\text{AuPH}_3)_3^+$ molecule, Pauli repulsion and the electrostatic

interaction decrease more than the increased orbital interaction, the aurophilic interaction exists.

When the $\text{O}(\text{CuPH}_3)_3^+$ molecule change the structure from D_{3h} to C_{3v} , ΔE is 0.40 kJ/mol. There is no cuprophilic interaction in C_{3v} structure for this molecule.

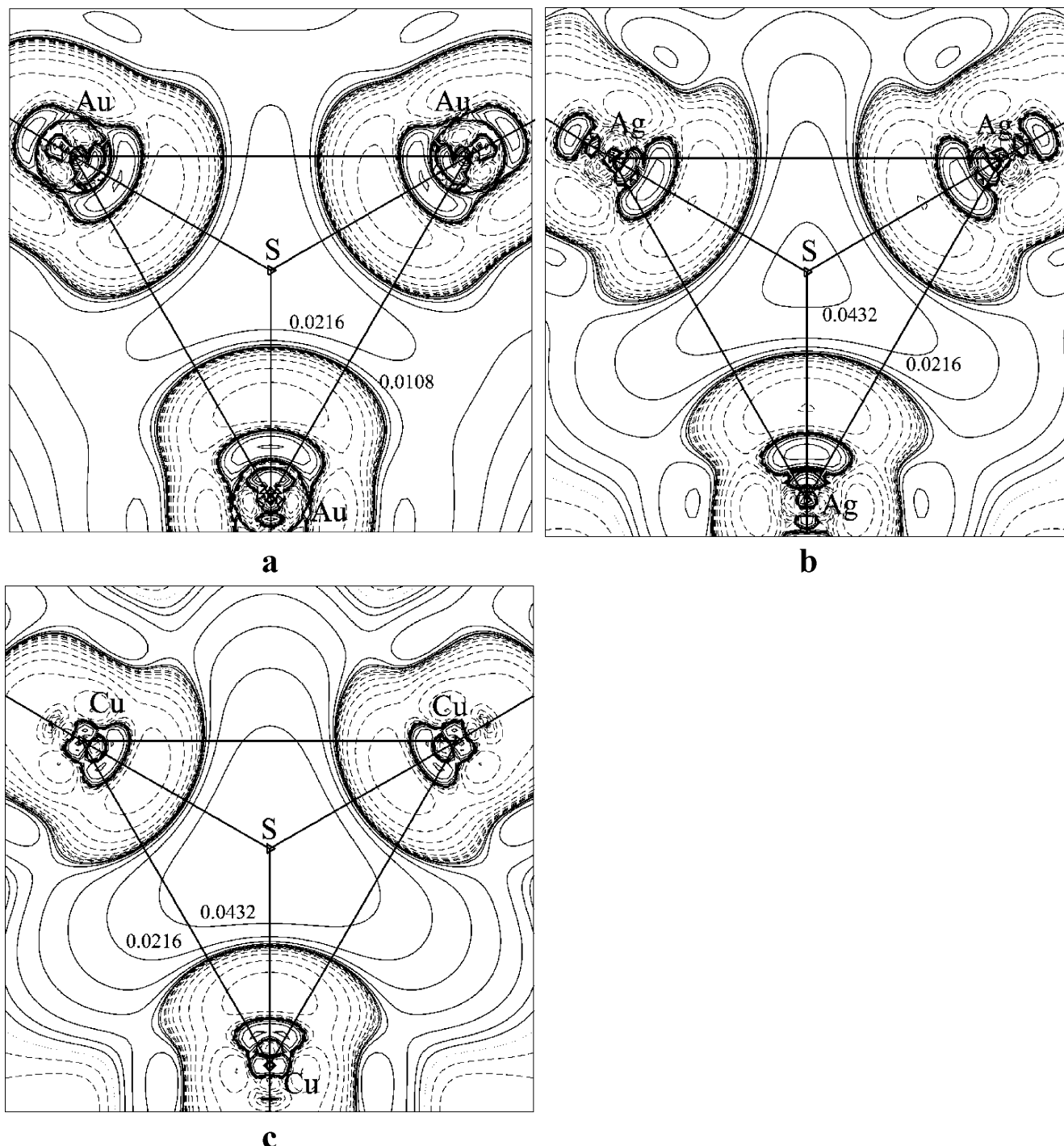


Fig. 6 Electron density difference $\Delta\rho$ ($e/\text{\AA}^3$) plots at $X\alpha/\text{TZ2P}$ level, **a**: $S(\text{AuPH}_3)_3^+$; **b**: $S(\text{AgPH}_3)_3^+$; **c**: $S(\text{CuPH}_3)_3^+$; along the plane of 3 Aus. Contour line values are $\pm 0.01 \times 2^n e\text{\AA}^{-3}$ ($n=0, 1, 2, \dots$); negative contour lines are dashed

Chemical deformation electronic densities

The electronic charge density distribution is a useful physical quantity that provides valuable information about the nature of bonding or nonbonding interactions in various molecular systems. The above mentioned density pattern is

exhibited both by the total electron density and by the difference density.

For the traditional difference density $\Delta\rho$, where averaged atomic ground state densities are subtracted from the molecular density, $\Delta\rho = \rho_{\text{mol}} - \sum \rho_{\text{atom}}$.

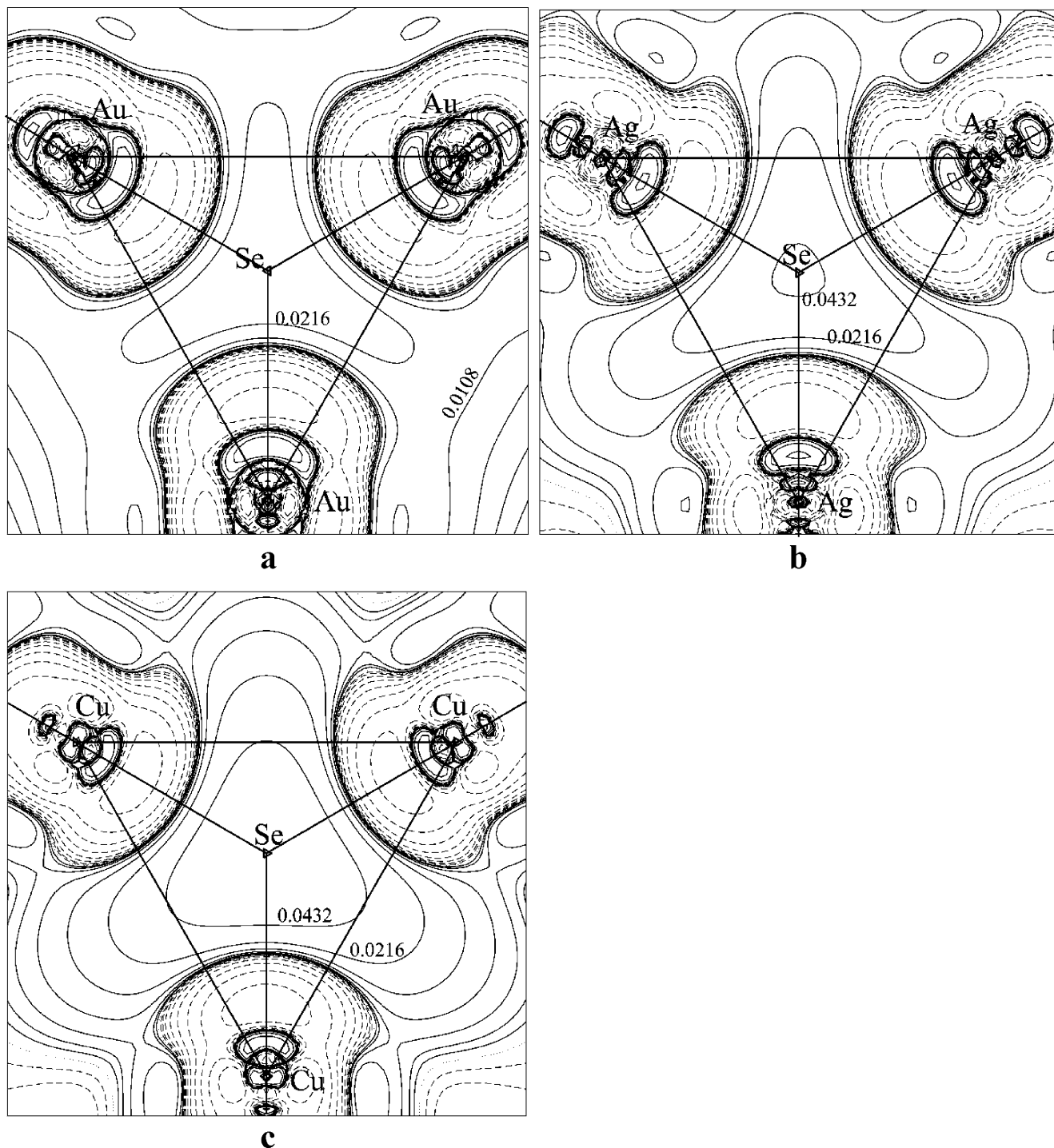


Fig. 7 Electron density difference $\Delta\rho$ ($e/\text{\AA}^3$) plots at $X\alpha/\text{TZ2P}$ level, **a**: $\text{Se}(\text{AuPH}_3)_3^+$; **b**: $\text{Se}(\text{AgPH}_3)_3^+$; **c**: $\text{Se}(\text{CuPH}_3)_3^+$; along the plane of 3 Aus. Contour line values are $\pm 0.01 \times 2^n e/\text{\AA}^3$ ($n=0, 1, 2, \dots$); negative contour lines are dashed

The original atomic charge distributions must be distorted in the formation of a molecule, and the distortion is such that charge density is concentrated on the binding region between the nuclear.

We show the difference density of the calculated $\text{X}(\text{MPH}_3)_3^+$ ($\text{X}=\text{O}, \text{S}, \text{Se}; M=\text{Au}, \text{Ag}, \text{Cu}$).

Figures 5, 6 and 7 show the electron density difference maps for $\text{X}(\text{MPH}_3)_3^+$ ($\text{X}=\text{O}, \text{S}, \text{Se}; M=\text{Au}, \text{Ag}, \text{Cu}$). Solid contours mean electron density increasing, dashed contours mean electron decreasing. As seen in Fig. 5, between the two $M(\text{I})$ atoms, the electron density increased 0.17 to $0.34 e/\text{\AA}^3$. For $\text{O}(\text{MPH}_3)_3^+$ ($M=\text{Au}, \text{Ag}, \text{Cu}$), since the

Table 6 Deviations ('estimated errors') $\overline{\Delta}$ of calculated aurophilic distances $R_{\text{Au...Au}}$, $R_{\text{Au-X}}$, $R_{\text{Au-P}}$ (in pm), $\theta_{\text{Au-X-Au}}$ (in degree) from experimental estimates of different compounds

Method	HF	MP2	X α	VWN	BP	PW91
$\overline{\Delta R}_{\text{Au-Au}}$	61.9	-13.9	-3.5	-6.3	20.1	29.5
$\overline{\Delta R}_{\text{Au-X}}$	4.8	0.9	-1.9	-1.6	2.6	1.7
$\overline{\Delta R}_{\text{Au-P}}$	11.9	3.2	-2.7	-3.7	0.2	0.8
$\overline{\Delta \theta}_{\text{Au-X-Au}}$	19.0	-6.9	-1.5	-2.8	5.4	9.7
$ \overline{\Delta R}_{\text{Au-Au}} $	61.9	13.9	3.7	6.3	20.1	29.5
$ \overline{\Delta R}_{\text{Au-X}} $	4.8	1.0	1.9	1.6	2.6	1.7
$ \overline{\Delta R}_{\text{Au-P}} $	11.9	3.2	2.7	3.7	0.6	0.6
$ \overline{\Delta \theta}_{\text{Au-X-Au}} $	19.0	6.9	3.2	2.8	7.9	12.1

metallophilic interaction is so small that the structure is close to the planar structure. So the raising electron density is the density of ionic bond M–X. For X(MPH₃)⁺ (X=S, Se; M=Au, Ag, Cu), there is about 0.02–0.04 e/Å³ electron density between the two M(I) atoms, just as seen in Figs. 6 and 7. We found that the electron density differences can not associate with the metallophilic interactions directly since they are not simply covalent systems.

The regions of charge increased (means the difference density increased) are, therefore, the regions to which charge is transferred relative to the separated atoms to obtain a state of electrostatic equilibrium and hence a chemical bond. We have just proven that the electron density redistributed in the process of forming the metallophilic interaction. From this point of view a density difference map provides us with a picture of the “bond density”.

Conclusion

In the present work, a series of central-atom gold complexes X(MPH₃)⁺ (X=O, S, Se; M=Au, Ag, Cu) have been studied by means of several density functional methods. The key conclusions may be summarized as follows.

The X α DFT methods used for the work reproduce the structural parameters of a few systems which were prepared experimentally fairly well (see Table 6). While MP2 method can not be appropriate to such closed-shell system (see also as Ref. [18]). When the metal is the same, the $R_{\text{X-M}}$ increases following the increase of the central atomic number. For the same central atom, relativistic bond length contraction effect causes that the $R_{\text{X-Au}}$ is shorter than $R_{\text{X-Ag}}$. $R_{\text{Au-P}}$ is shorter than $R_{\text{Ag-P}}$ because of the relativistic effect for the same central atom system. The metallophilic interactions to the systems have been required. For the X(MPH₃)⁺ (M=Au, Ag, Cu) system, when the central atom is S or Se, the aurophilic interaction is the strongest, and the cuprophilic interaction is the weakest. For the O(MPH₃)⁺ system, there is almost no metallophilic

interactions. Finally, the nature of metallophilic interaction is analyzed. For the structure from D_{3h} to C_{3v}, the decrease of the pauli repulsion converts into the aurophilic and argentophilic interaction.

Acknowledgment We acknowledge the financial supports by the National Nature Science Foundation of China (No. 20373041, 20573074).

References

1. Pyykkö P (1997) Chem Rev 97:597
2. Pathaneni SS, Desiraju GR (1993) J Chem Soc Dalton Trans 319
3. Grohmann A, Schmidbaur H (1995) In: Abel EW, Stone FG, Wilkinson AG (eds) Comprehensive organometallic chemistry II, vol 3. Elsevier, Oxford, UK, p 1
4. Scherbaum F, Grohmann A, Müller G, Schmidbaur H (1989) Angew Chem Int Ed Engl 28:463
5. Grohmann A, Riede J, Schmidbaur H (1990) Nature 345:140
6. Schmidbaur H, Weidenhiller G, Steigemann O (1991) Angew Chem Int Ed Engl 30:433
7. Zeller E, Schmidbaur H (1993) J Chem Soc Chem Commun 69
8. Zeller E, Beruda H, Kolb A, Bissinger P, Riede J, Schmidbaur H (1991) Nature 352:141
9. Canales F, Gimeno MC, Jones PG, Laguna A (1994) Angew Chem Int Ed Engl 33:769
10. Rösch N, Görling A, Ellis DE, Schmidbaur H (1989) Angew Chem Int Ed Engl 28:1357
11. Schmidbaur H, Steigemann O (1992) Z Naturforsch B 47:1721
12. Angermaier K, Schmidbaur H (1994) Inorg Chem 33:2069
13. Pyykkö P, Zhao Y (1991) Angew Chem Int Ed Engl 30:604
14. Pyykkö P, Li J, Runeberg N (1994) Chem Phys Lett 218:133
15. Magnko L, Schweizer M, Rauhut G, Schütz M, Stoll H, Werner HJ (2002) Phys Chem Chem Phys 4:1006
16. O'Grady E, Kaltsoyannis N, (2004) Phys Chem Chem Phys 6:680
17. Pyykkö P, Tamm T (1998) Organometallics 17:4842
18. Riedel S, Pyykkö P, Mata RA, Werner HJ (2005) Chem Phys Lett 405:148
19. Te Velde G, Bichelhaupt FM, Baerends EJ, Guerra CF, Van Gisbergen SJA, Snijders JG, Ziegler T (2001) J Comput Chem 22:931
20. Slater JC (1951) Phys Rev 81:385
21. Gaspar R (1954) Acta Phys 3:263
22. Schwarz K (1972) Phys Rev B 5:2466
23. Vosko SH, Wilk L, Nusair M (1980) Can J Phys 58:1200
24. Becke AD (1988) J Chem Phys 88:2547
25. Perdew JP (1986) Phys Rev B 33:8822

26. Perdew JP (1992) Phys Rev B 46:6671
27. Te Velde G, Baerends EJ (1992) J Comput Phys 99:84
28. Van Lenthe E, Ehlers AE, Baerends EJ (1999) J Chem Phys 110:8943
29. Van Lenthe E, Baerends EJ, Snijders JG (1994) J Chem Phys 101:9783
30. Van Lenthe E, Snijders JG, Baerends EJ (1996) J Chem Phys 105:6505
31. Van Lenthe E (1996) Int J Quan Chem 57:281
32. Häberlen OD, Rösch N (1993) J Phys Chem 97:4970
33. Guennic BL, Neugebauer J, Reiher M, Autschbach J (2005) Chem Eur J 11:1677
34. Angermaier K, Schmidbaur H (1995) Acta Crystallogr C51:1793
35. Schmidbaur H, Kolb AL, Zeller E, Schier A, Beruda H (1993) Z Anorg Allg Chem 619:1575
36. Angermaier K, Schmidbaur H (1994) Chem Ber 127:2381
37. Görling A, Rösch N, Ellis DE, Schmidbaur H (1991) Inorg Chem 30:3986
38. Wang SG, Schwarz WHE (2004) J Am Chem Soc 126:1266
39. Bowmaker GA, Schmidbaur H, Krüger S, Rösch N (1997) Inorg Chem 36:1754
40. Ziegler T, Snijders JG, Baerends EJ (1980) Chem Phys Lett 75:1
41. Ziegler T (1984) J Am Chem Soc 106:5901
42. Ziegler T, Rauk A (1977) Theo Chim Acta 46:1
43. Famiglietti C, Baerends EJ (1981) Chem Phys 62:407